

GEOMETRY OF THE CASIMIR EFFECT*

Roger BALIAN[†] and Bertrand DUPLANTIER[‡]

Service de Physique Théorique[§]

Orme des Merisiers, CEA-Saclay

F-91191 Gif-sur-Yvette Cedex

Abstract

When the vacuum is partitioned by material boundaries with arbitrary shape, one can define the zero-point energy and the free energy of the electromagnetic waves in it: this can be done, independently of the nature of the boundaries, in the limit that they become perfect conductors, provided their curvature is finite. The first examples we consider are Casimir's original configuration of parallel plates, and the experimental situation of a sphere in front of a plate. For arbitrary geometries, we give an explicit expression for the zero-point energy and the free energy in terms of an integral kernel acting on the boundaries; it can be expanded in a convergent series interpreted as a succession of an even number of scatterings of a wave. The quantum and thermal fluctuations of vacuum then appear as a purely geometric property. The Casimir effect thus defined exists only owing to the electromagnetic nature of the field. It does not exist for thin foils with sharp folds, but Casimir forces between solid wedges are finite. We work out various applications: low temperature, high temperature where wrinkling constraints appear, stability of a plane foil, transfer of energy from one side of a curved boundary to the other, forces between

* *Proceedings of the 15 th SIGRAV Conference on General Relativity and Gravitational Physics*, Villa Mondragone, Monte Porzio Catone, Roma, Italy, September 9-12, 2002; to appear in *Recent Developments in Gravitational Physics*, Institute of Physics Conference Series 176, Ed. Ciufolini et al, Oct 2004

[†]E-mail: balian@spht.saclay.cea.fr

[‡]E-mail: bertrand@spht.saclay.cea.fr

[§]Unité de recherche associée au CNRS 2306

distant conductors, special shapes (parallel plates, sphere, cylinder, honeycomb).

1 Introduction

1.1 A brief history

According to Planck (1900) [1], the energy of a stationary mode of the electromagnetic field (with frequency $\omega/2\pi$) is quantized with a contribution $\hbar\omega$ per photon. Because of the quadratic structure of the electromagnetic energy, a canonical transformation describes each mode as an harmonic oscillator. At the classical level, this representation was already known to Rayleigh, and Planck guessed rightly at the quantization of the oscillator energy levels. It was later discovered that their complete form reads

$$\varepsilon_N = \hbar\omega \left(N + \frac{1}{2}\right), \quad N \in \mathbf{N}, \quad (1)$$

with N the number of photons, and with a non-vanishing zero-point energy, $\frac{1}{2}\hbar\omega$, which reflects Heisenberg's uncertainty principle. One might have believed that the reference vacuum energy would be unobservable. Hendrik B G Casimir showed to the contrary in his famous 1948 article [2] that a physical force can be generated by vacuum fluctuations (see also [3], and for an historical account, [4]).

In its original form, the Casimir effect describes an attraction between two plane, parallel, perfectly conducting plates, which is explained by this occurrence of a virtual electromagnetic field in the vacuum separating the plates and in the vacuum lying outside them. Indeed, even when no real photon is present, the zero-point motion of each mode m of the field yields a contribution $\frac{1}{2}\hbar\omega_m(L)$ to the energy, which depends on the distance L between the plates. The variation with L of the overall zero-point energy manifests itself as the Casimir force. It is remarkable that, in spite of the divergence which appears when summing the zero-point energy over all modes, one finds a finite value for this force. Let us remark that a dimensional argument allows one to anticipate the right form of Casimir's result. A quantum pressure between two large plates should indeed depend on \hbar , c and on the distance L between them. To get pressure units $P \propto \text{N m}^{-2} = \text{J m}^{-3}$, with $\hbar \propto \text{J s}$, $c \propto \text{m s}^{-1}$, and $L \propto \text{m}$, one has first to multiply \hbar by c , so as to

eliminate time, and then divide by L^{-4} . Hence $P_{\text{Casimir}} \propto \frac{\hbar c}{L^4}$, and the real surprise is the finiteness of the numerical coefficient!

In recent experiments conducted in 1997-98 ([5, 6]), the Casimir force between a metallized sphere and a metallized plate was finally measured definitively with the help of atomic force microscopes. The field is nowadays the subject of intense research activity [7, 8]. Measurements of attractive Casimir forces are performed for the sphere-plane geometry [9], for micromechanical torsional devices [10], and for the original Casimir's planar geometry [11]. Lateral Casimir forces are measured between corrugated surfaces [12, 13] (see also [14]). Roughness effects are experimentally important ([15] and references therein). The experimental detection of temperature effects is an open problem [16].

1.2 Statement of the problem

It is somewhat puzzling to regard the Casimir effect as a property of vacuum containing a virtual electromagnetic field. It may look more natural to attribute it to the matter of the plates. Actually it is possible through Maxwell's equations to express the electromagnetic field, and hence its energy, in terms of the charge and current densities of the particles which can move within the conducting plates and which are the sources for the field. The zero-point motion of these particles then yields a non-vanishing interaction energy although the expectation values of the charge and current densities vanish. The force between the conducting plates at zero temperature can then be interpreted as a result of the interaction between the virtual zero-point currents that must exist in the ground state of matter owing to Heisenberg's inequality. However, this viewpoint is plagued by the fact that the interaction between charged particles is not instantaneous, but retarded. On the other hand, the evaluation of the force as a result of this interaction would rely on the specific structure of matter. In contrast, Casimir's viewpoint, which focuses on the field rather than on the matter of the plates, shows that the effect is nearly independent of the properties of matter (provided the plates are good conductors); moreover, as function of the electromagnetic field \mathbf{E} , \mathbf{B} the energy of this field at a given time is simply expressed as

$$\mathcal{E}_f = \frac{1}{2} \int d^3r [\epsilon_0 \mathbf{E}^2(r) + \mu_0^{-1} \mathbf{B}^2(r)] \quad (2)$$

in terms of the field at the same time, whereas $\mathbf{E}(r)$ and $\mathbf{B}(r)$ depend on the charges and currents at earlier times.

We wish to study the energy \mathcal{E}_f of the electromagnetic field in empty regions of space limited by boundaries with arbitrary shape, under circumstances when the expectation value $\langle \mathbf{E} \rangle, \langle \mathbf{B} \rangle$ of the quantum field vanishes at any point. The energy (2) may be non-zero for two reasons.

On the one hand, the uncertainty relations prevent the *quantum fluctuations* of \mathbf{E} and \mathbf{B} from vanishing, since these operators do not commute; hence the expression (2) for the energy has a positive minimum, the zero-point energy of the field. (We shall see that this value is not only strictly positive, but in fact infinite; however its variations are finite and physically meaningful.)

On the other hand, the vacuum where the field is considered is bounded by walls with which the field can be in thermodynamic equilibrium, at some temperature T . The field therefore presents random *thermal fluctuations* around its vanishing expectation value; they contribute to the energy (2) and to the entropy. We shall study this problem by evaluating the free energy of the field, wherefrom all thermodynamic equilibrium properties follow; in particular its variations with the shape provide the constraints on the walls at fixed temperature. This free energy includes the zero-point energy, to which it reduces at $T = 0$. We shall thus treat simultaneously the *Casimir effect* proper, associated with the *zero-point* energy, that is, to virtual photons, and the *radiation pressure* effects for a *black-body* with arbitrary shape, which are associated with real photons in equilibrium with the walls that act as a thermal bath.

Since general relativity is of no relevance in the present problem, energy is defined within an additive constant. We are interested only in its variations and can thus get rid of divergences in the theory by subtracting some constant that will tend to infinity.

We wish to define the Casimir effect as a property belonging only to the *field in vacuum*, independently of the nature of the material in the walls. In general the zero-point energy of a field depends on the matter to which this field is coupled. We shall use the term “Casimir effect”, in contrast to some authors, only when this energy can be defined separately. For electromagnetic fields within real materials, the interaction between the field and the charges does not allow us in general to separate out the energy (2) of the field alone; moreover the presence of a material affects the field even outside it. However, a complete decoupling is achieved in the limit of *perfectly*

conducting boundaries, which can be approached experimentally by use of *superconductors*. Both the electric and the magnetic fields \mathbf{E} and \mathbf{B} vanish inside them. Outside them, they simply impose the boundary conditions

$$\mathbf{E}_t = 0 \quad , \quad \mathbf{B}_n = 0 \tag{3}$$

on the tangential (t) and normal (n) components of the field. The presence of material bodies then has only a mere *geometric effect*. The part $-\int \mathbf{j} \cdot \mathbf{A}$ of the energy, which involves the currents and the vector potential and which determines the matter-radiation coupling in the equations of motion, can be assigned to the matter and left aside while \mathcal{E}_f is assigned to the vacuum. Anyhow, for perfect conductors, in a gauge where $\mathbf{E} = -\partial\mathbf{A}/\partial t$, this coupling energy vanishes on average since \mathbf{A} is perpendicular to the surface current \mathbf{j} .

In this idealized model, the field and the matter of the boundaries do not exchange any energy, even in time-dependent situations, although the coupling between the potentials and the charged particles relates \mathbf{E} and \mathbf{B} to the charge and current densities through Maxwell's equations of motion. Indeed, the rate of decrease of the energy (2) in some empty region of space is the outgoing flux of the Poynting vector $\mu_0^{-1}\mathbf{E} \times \mathbf{B}$ across the boundary of this region. The conditions (3) imply that the Poynting vector is tangent to a perfectly conducting wall, and hence that no energy can flow across such a wall. The establishment of thermal equilibrium in a vacuum is ensured only by the fact that real conductors are never perfect; this allows energy transfers between field and matter. Similarly to the model of an ideal gas, the present model is too crude to describe the establishment of equilibrium, but it is adequate for equilibrium properties.

1.3 Synopsis

We first recall Casimir's calculation for parallel plates, as well as its generalization to arbitrary temperatures. Through the further use of the so-called Derjaguin approximation, this allows us to briefly describe a recent experiment, and the irrelevance of temperature effects for the latter, allowing the conclusion that macroscopic quantum vacuum fluctuations are indeed observed at room temperature!

In the further study of arbitrary conductor geometries, we shall exhibit general aspects of the Casimir effect, for walls with arbitrary shape and at arbitrary temperatures. We wish to answer a few theoretical questions.

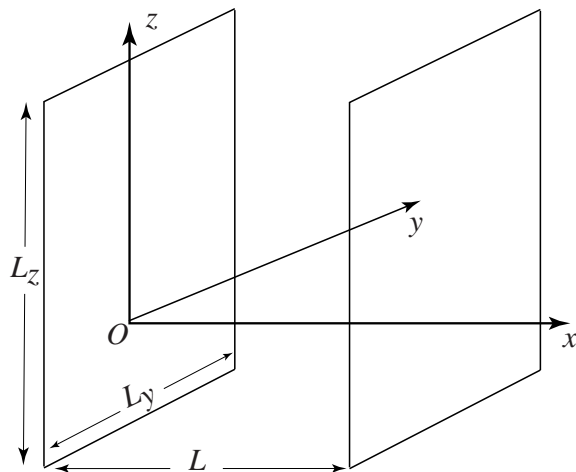


Figure 1: Conducting plates configuration.

Can the energy associated with the quantized electromagnetic field in the empty regions bounded by conducting walls be defined independently of the properties of these walls? How does it vary with the temperature of the photon gas that constitutes the field? Does the existence of the Casimir effect depend on the specific features of electromagnetism?

We shall rely on two detailed articles [17, 18] which deal with the above questions. This will allow us to leave aside the technicalities and to focus on the various ideas. The main result is embedded in section 5.5. For a bibliography on the Casimir effect we refer the reader to articles published in [8], and to recent monographs [7, 19, 20, 21, 22, 23, 24, 25].

2 Casimir's calculation (1948)

Consider two identical plates, parallel to the plane yOz , with a large area $\mathcal{A} = L_y \times L_z$, and separated by a distance L from each other along the orthogonal direction Ox .

The ideal plates are perfectly conducting, and the stationary modes are described by wave vectors (k_x, \mathbf{k}) , where $\mathbf{k} = (k_y, k_z)$ is parallel to the plates ; in the perpendicular direction, the boundary conditions give the discrete series: $k_x = \frac{\pi n}{L}$, where $n \in \mathbb{N}$, while periodic boundary conditions along the

plates* give $(k_y, k_z) = \left(\frac{2\pi n_y}{L_y}, \frac{2\pi n_z}{L_z} \right)$, where $n_y, n_z \in \mathbb{Z}$. This eigenmode, denoted by (n, \mathbf{k}) , oscillates with a “frequency” ω

$$\omega = \omega_n(\mathbf{k}) = c\sqrt{\frac{\pi^2 n^2}{L^2} + \mathbf{k}^2}. \quad (4)$$

Each eigenmode occurs with two possible polarizations (except for $n = 0$).

At zero temperature, the cavity electromagnetic energy is the sum \mathcal{E}_0 of the zero-point energies of the eigenmodes

$$\mathcal{E}_0 = \sum_{\text{modes } (n, \mathbf{k})} \varepsilon_0[\omega_n(\mathbf{k})], \quad \varepsilon_0(\omega) = \frac{1}{2}\hbar\omega. \quad (5)$$

The terms of this series are unbounded, and the series diverges. However, physics tells us how to cure this problem: at very high frequencies, the material ceases to conduct and becomes a dielectric, ultimately transparent to radiation. Then the boundary conditions no longer apply, and very high eigenmodes no longer contribute to the resulting force. This leads to introduce the mathematically convenient regularization

$$\mathcal{E}_0 = \sum_{\text{modes } (n, \mathbf{k})} \varepsilon_0[\omega_n(\mathbf{k})] \chi\left(\frac{\omega_n(\mathbf{k})}{\omega_c}\right), \quad (6)$$

where the cut-off function $\chi(\omega/\omega_c)$, is such that $\chi(0) = 1$, and is regular at the origin. It vanishes, along with all its derivatives, for $\omega/\omega_c \rightarrow +\infty$, sufficiently fast so that the sum converges. The cut-off frequency ω_c appears in χ for dimensional reasons ; it depends on the microscopic characteristics of the material. (The *perfect* conductor limit corresponds to $\omega_c \rightarrow +\infty$, so that $\chi(\omega/\omega_c) \rightarrow 1$ for any finite ω .)

For large values of L_y, L_z , one can replace the sums over *parallel* wave vectors by integrals. The distance L remains finite and associated with discrete modes. On thus gets

$$\sum_{\text{modes } (n, \mathbf{k})} \dots = 2 \frac{\mathcal{A}}{(2\pi)^2} \sum_{n=0}^{\infty} \int_{\mathbf{R}^2} d^2\mathbf{k} \dots, \quad (7)$$

*As usual, the asymptotic result does not depend on these boundary conditions.

where the *prime* means that the $n = 0$ mode has weight $1/2$. Let us define $\varepsilon(\omega) = \varepsilon_0(\omega) \chi(\omega/\omega_c)$. The energy (6) can then be written from (7)

$$\mathcal{E}_0(L) = 2 \frac{\mathcal{A}}{(2\pi)^2} \sum'_{n=0} \int_{\mathbf{R}^2} d^2\mathbf{k} \varepsilon[\omega_n(\mathbf{k})].$$

Owing to (4) one has, for n fixed, the form $\omega d\omega = c^2 k dk$, where $k = |\mathbf{k}|$. By simple integration over parallel wave vectors \mathbf{k} :

$$\int_{\mathbf{R}^2} d^2\mathbf{k} \varepsilon[\omega_n(\mathbf{k})] = 2\pi c^{-2} \int_{\omega_n(\mathbf{0})}^{+\infty} \omega d\omega \varepsilon(\omega), \quad \omega_n(\mathbf{0}) = \pi cn/L, \quad (8)$$

whence:

$$\mathcal{E}_0 = \mathcal{A} \frac{1}{\pi c^2} \sum'_{n=0} \int_{\pi cn/L}^{\infty} d\omega \omega \varepsilon_0(\omega) \chi\left(\frac{\omega}{\omega_c}\right). \quad (9)$$

The associated force, X_0 , can be readily derived,

$$X_0 = -\frac{\partial \mathcal{E}_0}{\partial L} = -\mathcal{A} \frac{\pi^2 \hbar c}{2L^4} \sum'_{n=0} g(n), \quad g(n) = n^3 \chi\left(\frac{\pi cn}{L\omega_c}\right). \quad (10)$$

The equivalent X_0^∞ of X_0 in the large L limit is given, as any continuum limit, by substituting the integral over n for the “primed” sum over n :

$$X_0^\infty = -\mathcal{A} \frac{\pi^2 \hbar c}{2L^4} \int_0^\infty dn g(n). \quad (11)$$

To obtain the zero-temperature force, associated with the vacuum energy $\varepsilon_0(\omega) = \frac{1}{2}\hbar\omega$, and acting on the plate, one must also take into account the opposite force exerted by the (infinite) electromagnetic vacuum *outside* of the capacitor. This force is just the opposite of (11), whence the resulting force

$$\tilde{X}_0 = X_0 - X_0^\infty = -\mathcal{A} \frac{\pi^2 \hbar c}{2L^4} \left[\sum'_{n=0} g(n) - \int_0^\infty dn g(n) \right].$$

To evaluate the difference between a series and the associated integral, we use the *Euler-Maclaurin* formula:

$$\sum'_{n=0} g(n) - \int_0^{+\infty} dn g(n) = -\frac{1}{12} g'(0) + \frac{1}{6!} g'''(0) + \mathcal{O}(g^{[5]}(0)), \quad (12)$$

which involves all g 's derivatives of odd order, taken at the origin, and which is valid for a function g vanishing at infinity, as well as all its derivatives. By calculating the successive derivatives, one finds here

$$g'(0) = 0, \quad g'''(0) = 6\chi(0) = 6, \quad g^{[p]}(0) = \mathcal{O}(\omega_c^{-(p-3)}), \quad p \geq 3.$$

One therefore finds the finite value[†]

$$\sum_{n=0}^{\infty} 'g(n) - \int_0^{\infty} dn g(n) = \frac{1}{5!} + \mathcal{O}(\omega_c^{-2}).$$

The zero-temperature resulting force thus possesses a universal limit for perfect conductors, i.e, when $\omega_c \rightarrow +\infty$. The limit pressure, found by H. B. G. Casimir in 1948, is:

$$\frac{1}{\mathcal{A}} \tilde{X}_0 = -\frac{\pi^2}{240} \frac{\hbar c}{L^4}. \quad (13)$$

The Casimir force is *attractive*, and one finds the analytic form which was anticipated in terms of \hbar , c and of the length L . Only the numerical coefficient remained to be found: $-\pi^2/240$, and the remarkable fact is that it is non-vanishing and *universal*, i.e., independent of the microscopic nature of the perfect conductors. To the resulting Casimir force is associated a *subtracted* zero-point energy $\tilde{\mathcal{E}}_0$ such that

$$\frac{1}{\mathcal{A}} \tilde{\mathcal{E}}_0 = -\frac{\pi^2}{720} \frac{\hbar c}{L^3}, \quad \tilde{X}_0 = -\frac{\partial \tilde{\mathcal{E}}_0}{\partial L}. \quad (14)$$

3 Electromagnetic free energy of a planar capacitor

3.1 Vacuum and thermal parts

Let us briefly consider the effect of temperature, in order to compare it to the zero-point effect[‡]. At a given temperature T , photons will fill in the cavity, and they obey the “black-body” statistics. To each classical eigenmode

[†]The presence of the factor n^3 , varying rapidly with n , yields the non-vanishing value $g'''(0) = 3!$. In the absence of such a term, the Euler-Maclaurin formula would start with $g'(0) = \mathcal{O}(\omega_c^{-1})$, and the difference between the sum and the integral would vanish in the perfect conductor limit.

[‡]The first calculations are due to Fierz [26] and Mehra [27].

(n, \mathbf{k}) is associated the Hamiltonian of a quantum harmonic oscillator, with frequency $\nu = \omega/2\pi$, $\omega = \omega_n(\mathbf{k})$, given by (4). The eigenvalues of this Hamiltonian are then $\varepsilon_N = \hbar\omega(N + 1/2)$, where $N \geq 0$ is the number of photons in the mode.

The free energy of an eigenmode ω at temperature T , with $\beta = 1/k_B T$, and k_B Boltzmann's constant, has the form

$$f(\omega) = -\frac{1}{\beta} \ln \sum_{N=0}^{\infty} e^{-\beta\hbar\omega(N+\frac{1}{2})} = \frac{1}{2}\hbar\omega + \frac{1}{\beta} \ln(1 - e^{-\beta\hbar\omega}). \quad (15)$$

We recast it as

$$f(\omega) = \varepsilon_0(\omega) + f_T(\omega), \quad (16)$$

with

$$\varepsilon_0(\omega) = \frac{1}{2}\hbar\omega, \quad f_T(\omega) = \beta^{-1}\varphi(\beta\hbar\omega), \quad (17)$$

where $f_T(\omega)$ is the *thermal* part of the mode free energy, and where

$$\varphi(x) = \ln(1 - e^{-x}), \quad \varphi(x) \leq 0.$$

By definition, the zero-temperature limit of $f_T(\omega)$ vanishes.

The purely thermal part of the electromagnetic free energy between the plates is then defined as follows:

$$\mathcal{F}_T = \sum_{(n, \mathbf{k}) \text{ modes}} f_T[\omega_n(\mathbf{k})]. \quad (18)$$

In contrast with the eigenmode sum associated with the vacuum, the sum (18) associated with the thermal radiation is *convergent*. By using (7) it can be written as

$$\mathcal{F}_T(L) = 2 \frac{\mathcal{A}}{(2\pi)^2} \sum_{n=0}^{\infty} \int_{\mathbf{R}^2} d^2\mathbf{k} \beta^{-1} \varphi[\beta\hbar\omega_n(\mathbf{k})]. \quad (19)$$

In (19) the integration over parallel vectors \mathbf{k} gives, as in (8):

$$\int_{\mathbf{R}^2} d^2\mathbf{k} \varphi[\beta\hbar\omega_n(\mathbf{k})] = 2\pi c^{-2} \int_{\omega_n(\mathbf{0})}^{+\infty} \omega d\omega \varphi(\beta\hbar\omega), \quad (20)$$

with $\omega_n(\mathbf{0}) = \pi n c/L$. In terms of the dimensionless variable $x = \beta \hbar \omega$, and of

$$\psi(u) = \int_u^{+\infty} dx x \varphi(x), \quad (21)$$

the free energy is obtained as a simple series:

$$\mathcal{F}_T(L) = 2 \frac{\mathcal{A}}{2\pi\beta} \frac{1}{(\beta\hbar c)^2} \sum_{n=0}^{\infty} {}' \psi(n\alpha), \quad \alpha = \beta\pi\hbar c/L. \quad (22)$$

3.2 Continuous limit

By comparing the energies $\hbar\omega$ of photons belonging to two consecutive eigenmodes, one can estimate the domain of temperatures T or separations L for which the discrete character of the eigenmodes disappears. For vanishing parallel wave vectors: $\hbar\Delta\omega = \hbar[\omega_{n+1}(\mathbf{0}) - \omega_n(\mathbf{0})] = \hbar\pi c/L = \alpha k_B T$, and the eigenmodes appear as a continuum for $\alpha \leq 1$. At ordinary temperature, $T \simeq 300$ K, this gives $L \geq 24 \mu\text{m}$, and only for shorter distances will the discrete character of the eigenmodes be detectable.

Let us introduce the large L limit, $\mathcal{F}_T^\infty(L)$, of the free energy $\mathcal{F}_T(L)$ (22). In the limit $\alpha = \beta\pi\hbar c/L \ll 1$, the series in \mathcal{F}_T converges towards the integral[§]

$$\mathcal{F}_T^\infty = 2 \frac{\mathcal{A}}{2\pi\beta} \frac{1}{(\beta\hbar c)^2} \frac{1}{\alpha} \int_0^{+\infty} du \psi(u).$$

The numerical coefficient is

$$\int_0^{+\infty} du \psi(u) = \int_0^{+\infty} dx x^2 \varphi(x) = -2\zeta(4) = -\frac{\pi^4}{45},$$

in terms of the Riemann ζ function. The continuum free energy

$$\mathcal{F}_T^\infty = -2 \frac{\mathcal{A}}{2\pi\beta} \frac{1}{(\beta\hbar c)^2} \frac{2}{\alpha} \zeta(4) = -\frac{\mathcal{A} L}{\beta} \frac{1}{(\beta\hbar c)^3} \frac{\pi^2}{45}, \quad (23)$$

[§]The presence of the ‘‘prime’’ notation in the sum over n and of the factor $\frac{1}{2}$ for the $n = 0$ mode are irrelevant in the large L limit. They imply a finite difference between the sums, which are here evaluated at order $\mathcal{O}(L)$ as integrals.

is precisely the *black-body free energy* in a large volume $\Omega = \mathcal{A} \times L$.

It is convenient to introduce the thermal *subtracted* free energy

$$\tilde{\mathcal{F}}_{\text{T}} = \mathcal{F}_{\text{T}} - \mathcal{F}_{\text{T}}^{\infty}, \quad (24)$$

which reads, owing to (22) and (23)

$$\tilde{\mathcal{F}}_{\text{T}} = 2 \frac{\mathcal{A}}{2\pi\beta} \frac{1}{(\beta\hbar c)^2} \left[\sum_{n=0}^{\infty} \psi(\alpha n) + \frac{2}{\alpha} \zeta(4) \right]. \quad (25)$$

3.3 Thermal forces

The force on, e.g., the right hand plate, is calculated as

$$X_{\text{T}}(L) = -\frac{\partial \mathcal{F}_{\text{T}}(L)}{\partial L}. \quad (26)$$

From the free energy (22) one finds

$$X_{\text{T}} = -2 \frac{\mathcal{A}}{2\pi\beta L} \frac{1}{(\beta\hbar c)^2} \sum_{n=0}^{\infty} n^2 \alpha^2 \varphi(n\alpha). \quad (27)$$

This force is perpendicular to the plate and positive ($\varphi(x) \leq 0$), hence repulsive. It is the black-body pressure in a finite geometry. In the $L \rightarrow \infty$ limit, one recovers the infinite volume black-body radiation pressure

$$X_{\text{T}}^{\infty} = -\frac{\partial \mathcal{F}_{\text{T}}^{\infty}}{\partial L} = \frac{\mathcal{A}}{\beta} \frac{1}{(\beta\hbar c)^3} \frac{\pi^2}{45}. \quad (28)$$

In fact, a given plate at temperature T is in equilibrium with the thermal radiation existing on both sides. It thus will also be subjected to the pressure force exerted by the exterior photons, which is just the infinite volume black-body pressure force, $-X_{\text{T}}^{\infty}$, that we just evaluated. The resulting thermal force is therefore:

$$\tilde{X}_{\text{T}} = X_{\text{T}} - X_{\text{T}}^{\infty} = -\frac{\partial (\mathcal{F}_{\text{T}} - \mathcal{F}_{\text{T}}^{\infty})}{\partial L} = -\frac{\partial \tilde{\mathcal{F}}_{\text{T}}}{\partial L}. \quad (29)$$

3.4 Short distance or low temperature expansion

The series (27) giving the interior thermal force X_T yields a natural *low-temperature* or *short-distance* expansion for $\alpha = \beta\pi\hbar c/L \gg 1$. Indeed the $n = 0$ term vanishes, and for $n \geq 1$, $\varphi(n\alpha) \sim -e^{-n\alpha}$. The $n = 1$ mode thus contributes a leading exponentially small repulsive force:

$$X_T = \mathcal{A} \frac{1}{\beta} \frac{\pi}{L^3} [e^{-\alpha} + \mathcal{O}(e^{-2\alpha})], \quad \alpha \gg 1.$$

In the thermal *resulting force* (29) \tilde{X}_T , the leading term will thus be the black-body exterior term:

$$\frac{1}{\mathcal{A}} \tilde{X}_T = -\frac{\pi^2}{45} \frac{1}{\beta} \frac{1}{(\beta\hbar c)^3} + \frac{1}{\beta} \frac{\pi}{L^3} [e^{-\alpha} + \mathcal{O}(e^{-2\alpha})]. \quad (30)$$

3.5 Comparison of zero-point and thermal effects

Adding (13) and (30), one gets the total pressure at low temperature or short distance:

$$\frac{1}{\mathcal{A}} X = \frac{1}{\mathcal{A}} (\tilde{X}_0 + \tilde{X}_T) = -\frac{\pi^2}{240} \frac{\hbar c}{L^4} - \frac{\pi^2}{45} \frac{1}{\beta} \frac{1}{(\beta\hbar c)^3} + \frac{1}{\beta} \frac{\pi}{L^3} e^{-\alpha} + \dots \quad (31)$$

Thus the resulting force is dominated by the Casimir and black-body forces, both attractive. For $L = 1\mu\text{m}$, indeed one gets $\alpha \simeq 24$. Hence the first internal mode contributes to the thermal force only with a relative factor e^{-24} !

The ratio $\gamma = \frac{\tilde{X}_T}{\tilde{X}_0}$ is thus, owing to (31): $\gamma \simeq -\frac{X_T^\infty}{\tilde{X}_0} = \frac{1}{3} \left(\frac{2\pi}{\alpha}\right)^4$. For $L = 500\text{ nm}$, $\alpha = 48$, one gets $\gamma = 0.98 \times 10^{-4}$. Thus even at room temperature, the vacuum fluctuations largely dominate the black-body effects. This is equivalent to a zero-temperature situation, and sensitive experiments will be able to detect the quantum vacuum effects.

3.6 Total free energy

Let us finally introduce the *total free energy* F associated with the vacuum energy and the thermal free energy[¶]

$$F \equiv \tilde{\mathcal{E}}_0 + \tilde{\mathcal{F}}_T = \tilde{\mathcal{E}}_0 + \mathcal{F}_T - \mathcal{F}_T^\infty. \quad (32)$$

[¶]In this total free energy the contribution of the exterior volume has been subtracted out. Its definition coincides with that of the regularized, then renormalized free energy given in sections 5.2 and 5.5 below. One has in particular: $F(0) = \tilde{\mathcal{E}}_0$, $F(T) - F(0) = \tilde{\mathcal{F}}_T$.

The total force acting on a plate is therefore

$$X = -\frac{\partial F}{\partial L}. \quad (33)$$

Using (14) and (25), we have

$$F = \mathcal{A} \frac{\pi^2 \hbar c}{L^3} \left[-\frac{1}{720} + \mathcal{G}(\alpha) \right], \quad (34)$$

$$\mathcal{G}(\alpha) = \frac{1}{\alpha^3} \left[\sum_{n=0}^{\infty} \psi(\alpha n) + \frac{2}{\alpha} \zeta(4) \right]. \quad (35)$$

The above series yields the natural low-temperature expansion of the thermal function \mathcal{G} is for $\alpha \gg 1$. Owing to definition (21)

$$\psi(0) = -\zeta(3), \quad \psi(\alpha) = -(\alpha + 1) [e^{-\alpha} + \mathcal{O}(e^{-2\alpha})], \quad \alpha \gg 1, \quad (36)$$

whence

$$F = \mathcal{A} \frac{\pi^2 \hbar c}{L^3} \left\{ -\frac{1}{720} + \frac{1}{\alpha^3} \left[-\frac{1}{2} \zeta(3) + \frac{2}{\alpha} \zeta(4) - (\alpha + 1) [e^{-\alpha} + \mathcal{O}(e^{-2\alpha})] \right] \right\}. \quad (37)$$

for $\alpha = \beta \pi \hbar c / L \gg 1$.

The high-temperature expansion can be obtained from (34) and the Poisson formula. One can also use a remarkable duality formula between low and high temperatures ^{||}[28]

$$\alpha^2 \mathcal{G}(\alpha) = \alpha'^2 \mathcal{G}(\alpha'), \quad \alpha \alpha' = (2\pi)^2, \quad (38)$$

which yields for the thermal free energy:

$$\tilde{\mathcal{F}}_{\text{T}}(L, \alpha) = (2\pi/\alpha)^4 \tilde{\mathcal{F}}_{\text{T}}(L, (2\pi)^2/\alpha). \quad (39)$$

From (37) we deduce the *high-temperature* limit of the total free energy:

$$F = -\mathcal{A} \frac{\zeta(3)}{8\pi\beta L^2} + \mathcal{O}\left(\beta^{-2} e^{-4\pi^2/\alpha}\right), \quad \alpha = \beta \pi \hbar c / L \ll 1. \quad (40)$$

^{||}This duality is valid only for parallel plates, see section 6.1 below.

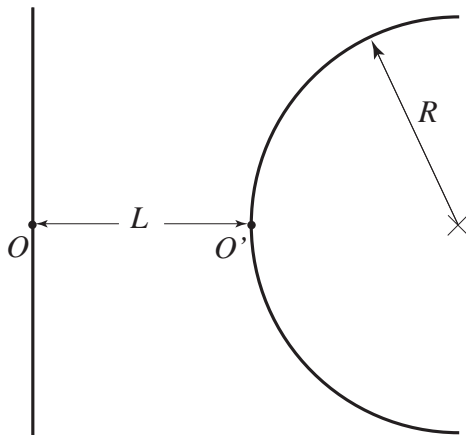


Figure 2: Experimental set-up of the conducting surfaces.

4 Force between a sphere and a plane

4.1 Experimental situation

An actual experimental set-up is described in Figure 2. A metallized sphere of radius R is placed in front of a conducting plate, at a distance $OO' = L$. In the experiments, like the one performed in 1998 [6], a polystyrene sphere is attached to the arm of an atomic force microscope, and placed in front of a polished planar surface. Their surfaces are coated with an aluminium layer a few hundred nanometers thick. To prevent corrosion, they are additionally coated with a very thin alloy layer, which is transparent to the radiation. The overall radius of the sphere is $R = 98.0 \pm 0.25 \mu\text{m}$. The range of distances is $120 \text{ nm} \leq L \leq 500 \text{ nm}$. Measures are performed at room temperature. Measurements with parallel plates, as in the original Casimir's calculation, are also performed [11], but are more difficult, due to the necessity to properly align the plates. This experimental problem is avoided in the sphere-plate geometry. However, the theoretical force is not explicitly known in this case, eventhough it exists in a closed form [18] (see sections 5.5 and 6.5.3 below).

4.2 Derjaguin approximation

An approximation method, due to Derjaguin (1934) [29], allows in the $L \ll R$ limit, the calculation of the sphere-plane interaction in terms of the purely

planar interaction. One replaces each elementary slice of the sphere cut parallel to the plane, by its orthogonal projection towards the plane. The resulting force then is

$$X^{\text{sph}}(L) = 2\pi R \int_L^{+\infty} \frac{1}{\mathcal{A}} X(x) dx, \quad (41)$$

where $X(x)$ is the force (33) between two planes at distance x . From (41) and definition (33) of X we immediately find

$$X^{\text{sph}}(L) = 2\pi R \frac{1}{\mathcal{A}} F(L), \quad (42)$$

where we used the fact that the total free energy F of two plates vanishes at infinity, as shown by the large-distance or high-temperature equivalent (40). The Casimir zero-point force on the sphere is thus:

$$X_0^{\text{sph}}(L) = 2\pi R \frac{1}{\mathcal{A}} \tilde{\mathcal{E}}_0(L) = -\frac{\pi^3}{360} R \frac{\hbar c}{L^3}, \quad (43)$$

where $\tilde{\mathcal{E}}_0$ is the Casimir energy (14) of two plates. For $R = 98.0 \pm 0.25 \mu\text{m}$, and for $L = 200 \text{ nm}$, one finds for example: $X_0^{\text{sph}} \simeq -33.4 \pm 0.09 \times 10^{-12} \text{ N}$. Such a force of the order of tens of pico-newtons is perfectly measurable, and comparable to forces implied in biological systems, e.g., in micromanipulations of single DNA macromolecules. In the experimental range $120 \text{ nm} \leq L \leq 500 \text{ nm}$, the minimal value of α is $\alpha_{\text{min}} = \alpha(L = 500 \text{ nm}) = 48$. Hence we can use the short-distance or low-temperature estimate (37) of the free energy F :

$$X^{\text{sph}}(L) = -\frac{\pi^3}{360} R \frac{\hbar c}{L^3} \left\{ 1 + 720 \left[\frac{1}{2\alpha^3} \zeta(3) - \frac{2}{\alpha^4} \zeta(4) + \mathcal{O}(\alpha^{-2} e^{-\alpha}) \right] \right\}. \quad (44)$$

The thermal correction in (44) is governed by the $\zeta(3)$ term, which gives in the experimental range ($L \leq 500 \text{ nm}$) a relative thermal correction 4×10^{-3} . It is attractive and adds to the leading zero-point term (43). Formula (44) is used by experimenters [6].

The simple zero-point formula (43) is shown in figure 3, in comparison with experimental results. The match is good, eventhough the experimental curve goes further above (43) at low values of L , with a relative shift in the tens of percents. This cannot be accounted for by temperature corrections

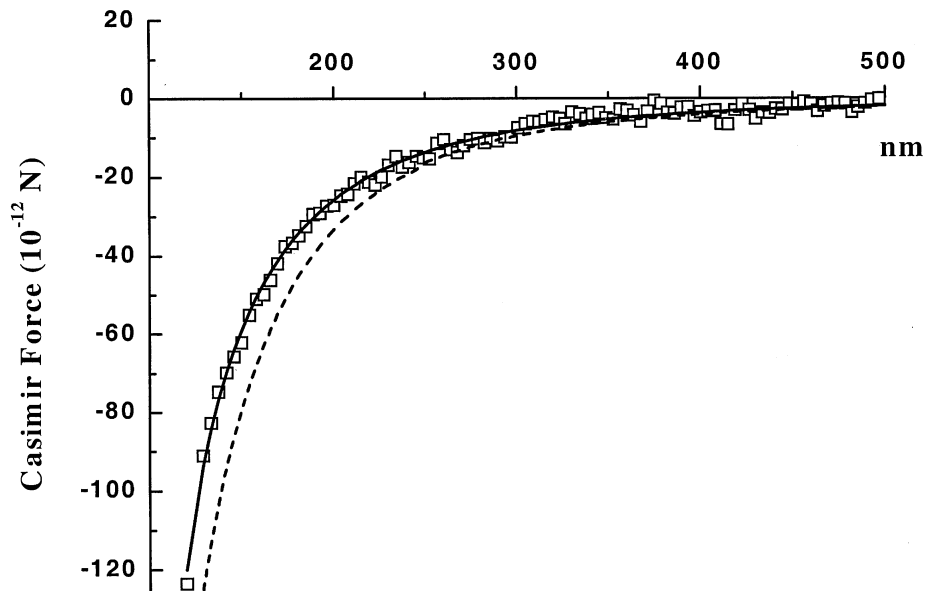


Figure 3: Comparison of the zero-point force (43) (dashed) with experimental results; the full curve takes into account finite conductivity and rugosity corrections (ref. [6]).

of order 10^{-3} , which furthermore lower the theoretical predictions. Good agreement ($\sim 1\%$) is found when finite conductivity and rugosity corrections are taken into account [6, 9, 30]. Let us also remark that the analysis of geometrical corrections to the Derjaguin approximation (41), following the general formalism described in the next sections, would be useful.

Before addressing the Casimir effect for arbitrary geometries, let us conclude that one does observe, even at room temperature, *macroscopic* electromagnetic forces, generated by vacuum fluctuations, and proportional to $\hbar c$, and *in the absence of charge and photons in the cavity!* ** Notice that several experiments also give clear evidence of retardation effects in atom-wall interactions, in agreement with the Casimir-Polder prediction [31].

**It is interesting to note that there is an infinity of longitudinal soft photons ($n = 0, \mathbf{k} \neq \mathbf{0}$) present in the cavity, but they do not contribute to the force; in contrast, photons with $n \geq 1$ are essentially absent from the cavity at such short separations L , which allows a direct observation of the vacuum energy, even at room temperature.

5 Arbitrary conductor geometries

5.1 Eigenmodes

Let us first consider a single connected region v limited by perfectly conducting boundaries. The electromagnetic field in v can be analyzed in terms of the eigenmodes m , obtained by solving Maxwell's equations

$$\begin{cases} \text{curl } \mathbf{E}_m = i\omega_m \mathbf{B}_m, & c^2 \text{ curl } \mathbf{B}_m = -i\omega \mathbf{E}_m, \\ \text{div } \mathbf{E}_m = 0, & \text{div } \mathbf{B}_m = 0, \end{cases} \quad (45)$$

with the boundary conditions (3). We shall keep aside the electrostatic and magnetostatic solutions with zero frequency, which do not contribute to the Casimir effect. Each mode m behaves as a harmonic oscillator with frequency $\nu_m = \omega_m/2\pi = cq_m/2\pi$ where q_m has the dimension of an inverse wavelength. Its associated energy (2) may take the quantized values $\varepsilon(q_m, N) = \hbar cq_m(N + \frac{1}{2})$. At finite temperature it yields a contribution $f(q_m)$ (15) to the free energy, which can also be written as (hereafter we use temperature units where $k_B = 1$)

$$f(q_m) = T \ln[2 \sinh(\hbar cq_m/2T)] . \quad (46)$$

At zero temperature the corresponding contribution to the energy of vacuum is $\frac{1}{2}\hbar cq_m$, the limit of (46) as $T \rightarrow 0$. For the high frequency modes such that $h\nu \gg T$, the free energy $f(q)$ is dominated by this zero-point energy. For the low frequency modes such that $h\nu \ll T$,

$$f(q) \sim -T \ln(T/\hbar cq) \quad (47)$$

is dominated by the classical $-T \ln T$ behavior.

The spectrum of eigenfrequencies, or equivalently of eigenwavenumbers $q_m^{(v)}$ in the considered region v is characterized by the *density of modes*

$$\rho^{(v)}(q) = \sum_m \delta(q - q_m^{(v)}) , \quad (48)$$

and the *free energy* of this region is formally equal to

$$F^{(v)} = \int_0^\infty dq \rho^{(v)}(q) f(q) . \quad (49)$$

A first difficulty arises if the domain v is infinite, since the spectrum is then *continuous*. We therefore imagine that the full system is enclosed in

a *large box* Σ , with volume V , which will eventually tend to infinity. By assuming this outermost boundary to be perfectly conducting, we not only discretize the spectrum m in the open regions v , but also confine the field and ensure that no energy is radiated outwards.

A second difficulty is associated with the fact that the spectra are *not bounded*. Indeed, for large q , the distribution (48) has the asymptotic expansion

$$\begin{aligned} \rho^{(v)}(q) \approx & \frac{v}{\pi^2} q^2 - \frac{2}{3\pi^2} \int \frac{d^2\alpha}{R} + \frac{1}{12\pi^2} \int ds \frac{(\pi - \theta)(\pi - 5\theta)}{\theta} \quad (50) \\ & + \mathcal{O}\left(\frac{1}{q^2}\right) + \mathcal{O}(q^{5/2} \times \text{osc}) . \end{aligned}$$

The dominant term is proportional to the *volume* v of the considered region; it is the only one which contributes to the black-body radiation in the thermodynamic limit. The second one is a *curvature* term; it is the integral over the boundaries of v of the average curvature $R^{-1} = \frac{1}{2}(R_1^{-1} + R_2^{-1})$, where R_1 and R_2 are the two main curvature radii at the point α , oriented towards the interior of v . It is supplemented, in case the boundary has not a finite curvature everywhere and includes wedges with a dihedral angle θ at the point s of the edge, by the next, *wedge* term, integrated along the wedge; we have for instance $\theta = \pi/2$ if v is the interior of a cube, $\theta = 3\pi/2$ if it is the exterior. Even if it is smoothed, the distribution (50) finally includes *oscillatory* terms with an amplitude which increases with $q^{\dagger\dagger}$. Since $f(q) \sim \frac{1}{2}\hbar cq$ for $q \rightarrow \infty$, all the terms exhibited in (50) lead to *divergences* in the free energy (49).

5.2 Regularization of the free energy

We encounter here the simplest example of the divergences that plague quantum field theory. We deal with them by using the standard technique. We first *regularize* the divergent formulae by means of *cut-offs*. We then deduce, from the resulting finite expressions, quantities that are physically *observable* at least theoretically. We finally *renormalize* these quantities by letting therein the cut-off parameters go to infinity. The theory is renormalizable if we get a finite limit for the physical quantities.

We have already regularized the “*infrared*” divergence associated with the infinite size of vacuum by introducing the *box* Σ . We shall deal with the

^{††}The corresponding semiclassical expansion of the density of modes over periodic orbits [17] has been recently experimentally tested in a superconducting microwave cavity [32]

“*ultraviolet*” divergence associated with the high frequencies $cq \rightarrow \infty$ in the integral (49) by introducing, as in section 2 above, a *cut-off factor* $\chi(q)$ close to 1 for $q \ll Q$ and decreasing sufficiently fast for $q \gg Q$ so as to restore convergence of the integral. Our final goal is to construct a renormalized free energy F , finite in the limit as $\Sigma \rightarrow \infty$, $Q \rightarrow \infty$. If this is feasible, it will mean that the ideal model of the electromagnetic field outside a set of perfectly conducting boundaries is renormalizable. In other words the Casimir effect exists as a property of the field proper, conditioned by the sole geometry of the boundaries S .

Let us first see how one can get rid of the most severe divergence, associated with the first term of (50) which after regularization with $\chi(q)$ yields $F^{(v)} \propto v\hbar cQ^4$. Consider, for instance, the Casimir force between two spheres with volumes v_1 and v_2 . There is here a single empty domain v_0 , which lies outside the spheres and inside Σ . Its volume is $v_0 = V - v_1 - v_2$. The only universal and natural way to cancel the corresponding divergence consists in replacing the solid conductors by *hollow thin conducting shells*, and in taking as a reference the free energy of the empty enclosure Σ , which is itself divergent. We now have three empty domains, v_0, v_1, v_2 , the volumes of which sum up to V . The most divergent term thus disappears if we subtract the free energy of the empty space within Σ from the total free energy in the presence of the two spherical shells, as

$$F^{(v_0)} + F^{(v_1)} + F^{(v_2)} - F^{(\Sigma)} . \quad (51)$$

More generally and more precisely (see Fig. 4), we denote as S the set of two-dimensional surfaces which bound the considered conductors. They partition the whole space (within the enclosure Σ) into a set of connected regions v , some of which coincide with the actual vacuum (as v_0 above), the other ones with the interiors of the conductors (as v_1 and v_2 above) . We then define the *regularized free energy* associated with the *whole space partitioned by S* as

$$F_{\text{reg}} = \int_0^\infty dq \left[\sum_v \rho^{(v)}(q) - \rho^{(\Sigma)}(q) \right] f(q)\chi(q) \equiv \int_0^\infty dq \delta\rho(q)f(q)\chi(q) . \quad (52)$$

This expression is finite owing to the cut-offs Σ and $\chi(q)$. If, as indicated above, it has a *finite limit* F as $\Sigma \rightarrow \infty$ and $\chi(q) \rightarrow 1$, independently of the shapes of Σ and $\chi(q)$, the Casimir effect will appear as a universal

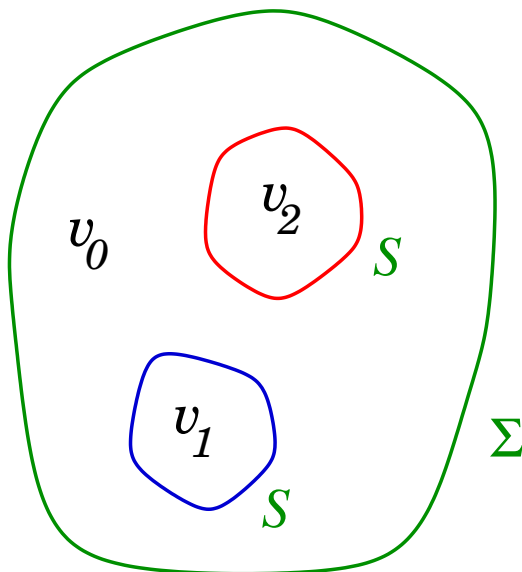


Figure 4: Set S of surfaces bounding the interiors v_1 and v_2 of conductors, and defining a third connected (vacuum) domain v_0 within enclosure Σ .

property characterized by the free energy F for the boundaries S , which will depend only on the *geometry of S* and on the temperature. This will provide us with a generating function for all mechanical and thermal properties in thermodynamic equilibrium, in two idealized circumstances.

On the one hand, the expression (52) can be directly interpreted as the change in the free energy of the vacuum when a system S of closed, extremely *thin conducting foils* is introduced. The variations of F under deformations of such foils determine the *constraints* induced on them by virtual (for $T = 0$) or real photons (for $T \neq 0$). For instance, for a single sphere separating two regions v_1 and v_2 , the dependence of (52) on the radius determines the pressure exerted on the skin of this hollow sphere by the internal and the external field. We shall also encounter below constraints which tend to corrugate such thin sheets, by studying how F changes under periodic deformations.

On the other hand, the expression (52) is also suited for the study of forces between *bulky indeformable conductors*, as we now show. Let us return to the above example of two spheres. After regularization the force between them is associated with the variation of $F^{(v_0)}$ when they are shifted apart. The regularized quantities $F^{(v_1)}$, $F^{(v_2)}$ which enter (51) are not physically

relevant to the present problem where we deal with bulky rather than empty spheres, but they do not depend on the distance between these two spheres. Actually, a perfectly conducting skin of a sphere behaves as a perfect screen and the electromagnetic fields, inside and outside, are independent. Thus the force evaluated from (51) is the same as that evaluated from $F^{(v_0)}$, and it is preferable to use (51) because the divergences are expected to be eliminated by this combination. More generally, whenever solid conducting bodies can be *displaced but not deformed*, we can derive the forces between them from the Casimir free energy (52) for which the interior of each body is replaced by vacuum. This trick will allow us to renormalize F . (However, for thermal properties, one should leave aside the contributions of real photons within the conductors.)

As mentioned above, the cut-off factor $\chi(q)$ which regularizes the integral (52) for large q has a physical meaning. At high frequency, real conductors are never perfect. Electromagnetic waves can penetrate them, and go freely across them if they are thin. The objects S become *transparent* and the modes within Σ tend to be the same, whether S is present or absent. Thus, for imperfect conductors, the factor $\delta\rho(q)$ in (52) would decrease for large q . In our model we simulate *imperfect conduction or transparency* at high frequency by evaluating $\delta\rho(q)$ for perfectly conducting sheets S and multiplying by $\chi(q)$.

We now proceed and study the behaviour of (52) when the boundary Σ is pushed away to infinity and when the conducting sheets S tend to become perfect with $\chi(q) \rightarrow 1$.

5.3 Fields in the presence of perfect conductors

Our strategy will rely on the following ideas.

- (i) We replace the solution of eqs. (3), (45), which define the modes in each region v , by the determination of the *Green functions* associated with these partial differential equations and boundary conditions. Such a Green function contains in a synthetic way the whole information on the modes. It is a function of a complex variable k , *analytic* in the upper half-plane.
- (ii) We express the distribution of modes $\rho^{(v)}(q)$ in terms of the *boundary value* for $k \rightarrow q + i0$ of the Green functions.

- (iii) This will allow us to regard (52) as an integral in the complex plane k along the half-line $k = q + i0$, $q > 0$, and to *deform this contour* towards the pure imaginary axis $k = iy$, $y > 0$ where the Green functions are more regular than along the real axis (they have an infinity of poles at $k = \pm q_m$).
- (iv) We determine the Green functions by means of *Neumann's method*, which expresses them as solutions of two-dimensional integral equations over the boundaries S and Σ . The regularized free energy will thereby be expressed through the kernel of these integral equations in terms of the geometry of S and Σ .
- (v) Along the new integration contour $k = iy$, we can solve these integral equations by *iteration*. The resulting series are convergent, and can be interpreted physically as describing *multiple scattering* of an electromagnetic wave on the walls, involving *successively induced currents*.
- (vi) Convergence of the multiple scattering expansion allows us finally to control the limit $\Sigma \rightarrow \infty$, $\chi \rightarrow 1$ and to find an explicit expression for the limit F of (52).

We shall content ourselves here with a sketch of this programme. Detailed proofs can be found in [17, 18]. Given the symmetry between the fields \mathbf{E} and \mathbf{B} in eqs.(45), it is convenient to introduce *two Green functions*, a *magnetic* one $\mathbf{\Gamma}(r, r')$ and an *electric* one $\mathbf{\Xi}(r, r')$, which are tensors with two indices at r and r' . The first one represents the magnetic field created at the point r , in the presence of the conducting boundaries S and Σ , by a magnetic dipole lying at r' and oscillating as e^{-ickt} at the complex frequency $ck/2\pi$. The current density associated with this source is (within the factor μ_0)

$$\mathbf{j}_0(r, r') = \text{curl}_r [\delta^3(r - r')\mathbf{1}] \quad (53)$$

where $\mathbf{1}$ is the unit tensor. In each region v , $\mathbf{\Gamma}(r, r'; k)$ is the solution of the partial differential equation

$$(\nabla^2 + k^2)\mathbf{\Gamma} = -\text{curl } \mathbf{j}_0 \quad , \quad \text{div } \mathbf{\Gamma} = 0, \quad (54)$$

obtained by eliminating \mathbf{E} from the eqs.(45), with the boundary conditions

$$\mathbf{\Gamma}_n = 0 \quad , \quad (\text{curl } \mathbf{\Gamma})_t = 0. \quad (55)$$

The Green function $\mathbf{\Gamma}(r, r')$ is the magnetic field generated at the point r by the source \mathbf{j}_0 at r' and the currents $\mathbf{j}(\alpha, r')$ that it induces at the points α of the conducting surfaces S, Σ . We shall denote as n_α the normal vector at α , oriented towards the region v where r and r' lie. Both \mathbf{j}_0 and \mathbf{j} are tensors with two indices; the first one refers to the direction of the current, the second one to the orientation of the dipole at r' . Using the formalism of retarded potentials, we can express the magnetic field created by each elementary current \mathbf{j} as $M\mathbf{j}$, where M is the kernel

$$M(r, r') = \text{curl}_r [G_0(|r - r'|)\mathbf{1}] . \quad (56)$$

A product like $M\mathbf{j}$ stands for integration over space and summation over a tensor index. The scalar Green function

$$G_0(r) = \frac{e^{ikr}}{4\pi r} \quad (57)$$

is the solution of the equation $(\nabla^2 + k^2)G_0(r) = -\delta^3(r)$ that vanishes at infinity for $\text{Im}k > 0$. The magnetic Green function $\mathbf{\Gamma}$ is thus expressed as

$$\mathbf{\Gamma}(r, r') = \int d^3r'' M(r, r'') \mathbf{j}_0(r'', r') + \int_{S, \Sigma} d^2\alpha M(r, \alpha) \mathbf{j}(\alpha, r') ; \quad (58)$$

its first term $\mathbf{\Gamma}_0$ is the field produced by the dipole (53) in the infinite space. The as yet unknown currents \mathbf{j} satisfy the integral equation on the boundary

$$\mathbf{j} = \mathbf{j}_1 + K\mathbf{j} \quad , \quad \mathbf{j}_1(\alpha, r') = \int d^3r K(\alpha, r) \mathbf{j}_0(r, r'), \quad (59)$$

where the kernel K between two points α and β of the boundary is the tensor

$$K(\alpha, \beta) = 2n_\alpha \wedge \text{curl}_\alpha [G_0(|\alpha - \beta|)\mathbf{1}]. \quad (60)$$

In eq.(59) the product $K\mathbf{j}$ stands for summation on the tensor index and integration over α on the boundary. The proof of (59), (60) relies on an extension of Neumann's method, based upon the discontinuity of the surface integral in (58) when r crosses the boundary [18].

Altogether the solution of (59) determines \mathbf{j} , and $\mathbf{\Gamma}$ follows from (58), taking into account the various definitions (53), (56), (57), (60). The solution of the partial differential equation (54) with the boundary conditions (55) thus amounts to the solution of the *integral equation (59) on the boundary*.

The Green function $\mathbf{\Gamma}$ is a *generating function for the modes* m defined by (3), (45) in the connected region v where the source (53) lies. Indeed, in terms of the complex variable k , its poles are the real points $k = \pm q_m = \pm \omega_m/c$ and the corresponding residues are given by

$$\mathbf{\Gamma}(r, r'; k) = \sum_m \frac{q_m^2}{q_m^2 - k^2} \mathbf{B}_m(r) \otimes \mathbf{B}_m(r') , \quad (61)$$

where the magnetic field $\mathbf{B}_m(r)$ for the mode m is the real solution of (3), (45), normalized according to $\int_v d^3r \mathbf{B}^2(r) = 1$. The *spectral density* (48) is thus related to $\mathbf{\Gamma}$ through

$$\rho^{(v)}(q) = \frac{2}{\pi q} \int_v d^3r \operatorname{tr} \operatorname{Im} \mathbf{\Gamma}(r, r; q + i0) , \quad (62)$$

where the trace tr refers to the tensor indices.

We can likewise introduce an *electric Green function* $\mathbf{\Xi}$ by interchanging magnetic and electric fields, which amounts to interchanging the boundary conditions (55). It is the electric field created at the point r by a source with current density $\operatorname{curl} \mathbf{j}_0 / ick$ in the presence of the boundaries S, Σ . Taking (53) into account, we see that, except at $r = r'$, this source produces the same electric field as an electric dipole with current density $-ik[\delta^3(r - r')\mathbf{1}]/c$.

Provided r and r' lie in the same region v , the electric Green function $\mathbf{\Xi}(r, r'; k)$ can be represented by an expression analogous to (58), (59), within the mere *change in sign of \mathbf{j}_1* . (However, whereas $\mathbf{\Gamma}$ is expressed by means of (58) in terms of a true electric current density, the similar expression for $\mathbf{\Xi}$ involves a fictitious current, without physical meaning. Moreover, if we take r and r' on different sides of a boundary S , the expression (58) for $\mathbf{\Gamma}$ vanishes as it should, whereas the similar representation for $\mathbf{\Xi}$ provides an unphysical non-zero value. Such a behaviour is currently found in the books of mathematics that deal with Neumann's method; in fact, paradoxically, single-layer potentials are used there to represent Green functions when they vanish on the boundary, double-layer potentials when their normal derivative vanishes, whereas it is natural in electrostatics to make the converse choice. It is the application of Neumann's method in two different ways which allowed us to find the above simple relation between the representations of $\mathbf{\Gamma}$ and $\mathbf{\Xi}$.)

Since $\mathbf{\Xi}$ has the same spectral representation (61) as $\mathbf{\Gamma}$ within the replacement of \mathbf{B}_m by \mathbf{E}_m , we can equivalently express the distribution of

eigenmodes (62) as

$$\rho^{(v)}(q) = \frac{1}{\pi q} \int_v d^3r \operatorname{tr} \operatorname{Im}[\mathbf{\Gamma} + \mathbf{\Xi}(r, r; q + i0)] , \quad (63)$$

and simplifications will appear owing to this combination.

In fact, the *iteration* of the integral equation (59) provides

$$\mathbf{j} = \mathbf{j}_1 + K\mathbf{j}_1 + K^2\mathbf{j}_1 + \cdots , \quad (64)$$

a series which exhibits the surface current \mathbf{j} as the sum of *successively induced currents*: \mathbf{j}_1 is according to (59) a current directly induced by the dipolar source on the conducting boundaries; it induces in turn through the propagator K a secondary current $K\mathbf{j}_1$, and so on. The expression (60) of K and the behaviour of the free Green function (57) show that this propagator decreases exponentially at large distances (while oscillating) for $\operatorname{Im}k > 0$. Moreover, $K(\alpha, \beta)$ vanishes when the point β lies in the plane tangent at α to the boundary. Thus a current circulating on a plane boundary does not induce through K any secondary current on the same plane. At short distances K vanishes for a smooth boundary and is proportional to its curvature; this ensures the convergence of the integrals in $K\mathbf{j}_1$, $K^2\mathbf{j}_1$, etc. By relying on these properties, we can show that the expansion (64) is *convergent* at least in the region $\operatorname{Im}k > |\operatorname{Re}k|$. (For $k = 0$ describing static fields, the convergence depends on the *topology* of the boundaries.) The general theory of the Casimir effect will make use of this convergence.

The series for $\mathbf{\Gamma}$ which results from (58) and (64) reads

$$\mathbf{\Gamma} = M \frac{1}{1 - K} \mathbf{j}_0 = M \mathbf{j}_0 + MK \mathbf{j}_0 + MK^2 \mathbf{j}_0 + MK^3 \mathbf{j}_0 + \cdots , \quad (65)$$

where M defined by (56) describes the propagation of a wave issued from a unit element of current, and where K defined by (60) describes a similar propagation followed by the creation of an induced current. We can thus interpret (65) as a *multiple scattering expansion*: the wave issued from the source at r' may reach directly r (first term); it may propagate from r' to a point α of the boundary where it is scattered to reach r (second term); it may scatter successively twice on the boundary before reaching r (third term); and so on. The grazing scatterings vanish, so that the series (65) reduces to its first two terms for a single plane boundary, the second one describing the reflected wave.

The electric and magnetic Green functions are related to each other through

$$\Xi(r, r'; k) = k^{-2} \text{curl}_r \text{curl}_{r'} [\Gamma(r, r'; k) - \Gamma(r, r'; 0)], \quad (66)$$

and conversely. However the alternate series

$$\Xi = M \frac{1}{1+K} \mathbf{j}_0 = M \mathbf{j}_0 - MK \mathbf{j}_0 + MK^2 \mathbf{j}_0 - \dots, \quad (67)$$

which results from the integral equation over S, Σ for Ξ does not correspond term by term to (65), (66).

This expansion has the same interpretation in terms of successive scatterings as (65) in the physical situation when r and r' lie in the same connected region v . (However, if r and r' lie in two different regions v separated by a boundary S , the series (67) converges towards some non-zero value, and thus does not represent the actual electric field produced at r by the source at r' . On the contrary the various terms of the expansion (65) interfere destructively in such a configuration.)

Adding (65) and (67) as in (63) cancels all the odd terms of the expansion and yields a geometric series in K^2 . Only survive in the evaluation of the distribution of modes the terms describing an *even number of scatterings*. On the other hand, in the summation over the regions v , we shall have to transfer the two points r and r' (with $r = r'$) from one side to the other of the surface S . The kernel K changes its sign in this operation, since its definition (60) involves the normal vector n_α oriented in the direction of the domain v where the Green function is evaluated. After addition of Γ and Ξ in (63), the eigenmodes on both sides of S are evaluated with the *same integrand*. This remark will allow us to perform explicitly the summation over v and the integration over r in (68) below.

5.4 Limiting process

We are now in position to express the regularized free energy (52) in terms of the kernel K on the boundaries S, Σ . In order to switch the integration over q towards the complex plane k , we introduce the *generating function of the modes*:

$$\delta\Phi(k) = \frac{1}{2} \int d^3r \text{tr} \lim_{r' \rightarrow r} \left[\sum_v (\Gamma^{(v)} + \Xi^{(v)}) - \Gamma^{(\Sigma)} - \Xi^{(\Sigma)}(r, r'; k) \right]. \quad (68)$$

As in (51) or (52), we have summed over the various regions v bounded by S and enclosed in Σ , and subtracted the contribution of the empty box; the integral is therefore carried over the whole interior of Σ . The Green functions are singular for $r' \rightarrow r$, but their singular part, which arises only from the first term $\mathbf{\Gamma}_0(r-r') = \mathbf{\Xi}_0(r-r') = M\mathbf{j}_0$ of (33) and (35), is cancelled in (68) by the subtraction of $\mathbf{\Gamma}^{(\Sigma)} + \mathbf{\Xi}^{(\Sigma)}$. Thus no divergence appears in (68).

Like the $\mathbf{\Gamma}$ and $\mathbf{\Xi}$'s, the function $\delta\Phi(k)$ has no other singularity than poles at the points $k = \pm q_m$ of the real axis, with residues $\mp \frac{1}{2}q_m$. Hence, according to (63), we have

$$\delta\rho(q) = \frac{2}{\pi} \text{Im} \delta\Phi(q + i0) \quad (69)$$

for $q > 0$. The expression (46), (52), (69) of the regularized free energy thus reads

$$F_{\text{reg}} = \frac{2T}{\pi} \text{Im} \int_0^{\infty+i0} dk \frac{\delta\Phi(k) - \delta\Phi(i0)}{k} \ln \left(2 \sinh \frac{\hbar ck}{2T} \right) \chi(k) . \quad (70)$$

The subtraction of the real number $\delta\Phi(i0)$, which is equal to $\delta\Phi(0)$ when the box Σ is finite, ensures the convergence of the integral; it corresponds to the fact that static fields associated with $k = 0$ do not contribute to the Casimir effect.

In order to take advantage of the convergence of the expansions (65) and (67) for $\text{Im}k > |\text{Re}k|$ in (68), (70), we shall deform the integration contour in (70) towards the imaginary axis. We also *get rid of the spatial cutoff* Σ . We therefore introduce the function

$$\Psi(y) = \lim_{\Sigma \rightarrow \infty} \delta\Phi(iy) . \quad (71)$$

When taking the limit $\Sigma \rightarrow \infty$, we note that G_0 defined by (57) and hence M and K defined by (56) and (60) decrease exponentially with the distance l as e^{-yl} . The function $\Phi(iy)$ is represented, through its definition (68) and the multiple scattering expansions (65), (67), by *closed paths* that bounce an *even* number of times on S or Σ . All paths which involve only scatterings on Σ are compensated for, owing to the subtraction in (68). The contributions of all the paths which involve at least one back and forth travel between S and Σ contain a factor e^{-2yL} where L is the minimum distance from S to Σ ; they disappear when Σ is pushed away to infinity. The remaining paths which contribute to $\Psi(y)$ involve only scatterings on S , in even number;

before integration over $r' = r$ of (68) they contain for large r a factor e^{-2yL} , where L is the shortest distance between r and S , so that the integral over r is convergent. We shall perform it explicitly below. Note that the poles on the real axis of $[\delta\Phi(k) - \delta\Phi(i0)]/k$ with residues $\pm\frac{1}{2}$, above which the integral (70) runs, become dense in the limit $\Sigma \rightarrow \infty$ and are replaced by a cut.

It remains to *get rid of the ultraviolet cutoff* $\chi(k)$ which eliminates the high frequencies. In order to deform the contour of (70) towards the half line $k = iy, y > 0$ where the singularities of the logarithm lie, we take for $\chi(k)$ a meromorphic function of the form

$$\chi(k) = \sum_i \frac{a_i}{k^2 - \mu_i^2} + \frac{a_i^*}{k^2 - \mu_i^{*2}} . \quad (72)$$

The poles μ_i lie in the first quadrant and their residues satisfy

$$\sum_i \operatorname{Re} a_i = 0 , \quad -2 \sum_i \operatorname{Re}(a_i/\mu_i^2) = 1 . \quad (73)$$

The moduli $|\mu_i|$ have the same order of magnitude as a number Q that will tend to infinity, so that $\chi(q)$ is close to 1 as long as $q \ll Q$ and decreases as q^{-4} when $q \gg Q$. This behaviour ensures the convergence of (52) on account of the behaviour of the residual terms in (50).

Deforming the contour of (70) towards the imaginary axis produces terms associated with the residues at the points $k = \mu_i$. The properties of $\delta\Phi(k)$ then ensure that these residues vanish when $|\mu_i| \propto Q \rightarrow \infty$.

Indeed, for $k \rightarrow \infty$ in the first quadrant, it turns out that the multiple scattering expansion (65), (67) is dominated by its lowest, two-scattering term $MK^2\mathbf{j}_0$, provided the surface S is twice differentiable. The result is found from a short-distance expansion as

$$\Psi(y) = \frac{1}{32\pi} \int_S d^2\alpha \left(\frac{1}{R_1 R_2} - \frac{3}{R^2} \right) + \mathcal{O}\left(\frac{1}{y^2}\right) , \quad (74)$$

where R_1 and R_2 are the two principal curvature radii and $1/R$ the average curvature at the point α . Finally, near the origin, Ψ behaves as

$$\Psi(y) \approx -n(1 - Ay) + \mathcal{O}(y^2) , \quad (75)$$

where n is the genus of S , depending only on its topology ($n = 0$ for a sphere, $n = 1$ for a torus), and where $A > 0$.

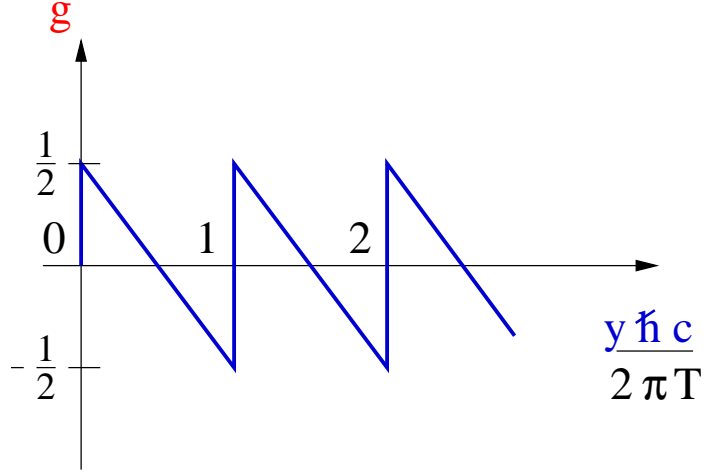


Figure 5: Sawteeth function g (77) drawn as a function of the dimensionless variable $y/\eta = y\hbar c/2\pi T$.

5.5 The renormalized casimir free energy

Altogether, using the above properties, we find the limit of (52) for $\Sigma \rightarrow \infty$ and $Q \rightarrow \infty$ or $\chi(q) \rightarrow 1$ as

$$F = \frac{\hbar c}{\pi} \int_0^\infty dy [\Psi(y) - \Psi(\infty)] + 2T \int_0^\infty \frac{dy}{y} [\Psi(y) - \Psi(+0)] g(y), \quad (76)$$

where the *temperature* appears through the sawteeth function

$$g(y) = \frac{1}{2} - \frac{y}{\eta} + \sum_{n=1}^{\infty} \theta(y - n\eta), \quad \eta = \frac{2\pi T}{\hbar c}. \quad (77)$$

with $\theta(x) = 0$ for $x < 0$, $\theta(x) = 1$ for $x > 0$. A closed expression for the function $\Psi(y)$, which encapsulates the effect of the *geometry* of the boundaries S on the modes of the field, is found by integrating (68) on r in the whole space. We noted that its integrand is the same for all the regions v separated by S , so that this integral depends only on the first and last scattering points on S in the expansions (65), (67). The integration over $r = r'$ of the corresponding product of M and $K\mathbf{j}_0$ can be expressed only in terms of the kernel K on S , and it simply yields $\frac{1}{2}y dK/dy$. Hence we find

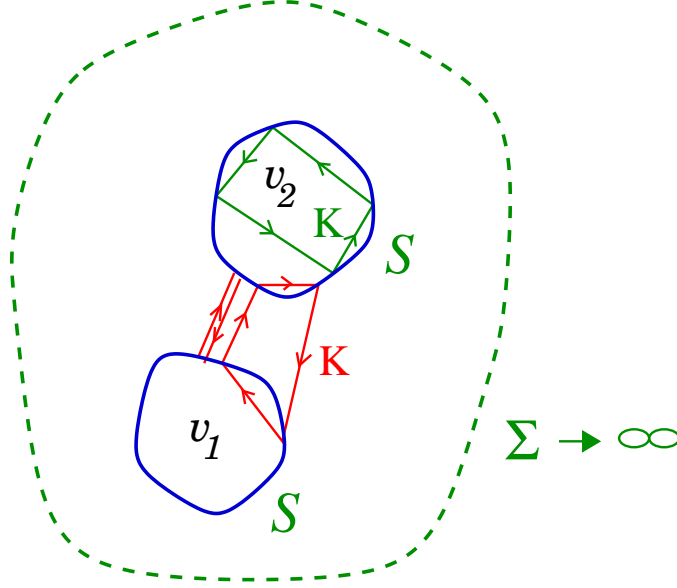


Figure 6: Closed paths (all with an even number of segments) contributing to the operator trace $\text{Tr} \ln(1 - K^2)$ in the function Ψ (78). Multiple scattering on a single shell contributes to the self-energy, while scattering between two surfaces contributes to their mutual energy. The enclosure Σ (dotted line) has been taken to ∞ .

$$\Psi(y) = -\frac{y}{4} \frac{d}{dy} \text{Tr} \ln(1 - K^2) , \quad (78)$$

where the trace Tr and the products stand for integration over S of a variable α and summation on the tensor indices of K (see Fig. 6). Expressed as function of y , the kernel K on the surface S defined by (57), (60) reads

$$K(\alpha, \beta; y) = \frac{1}{2\pi} n_\alpha \wedge \text{curl}_\alpha \left[\frac{e^{-y|\alpha-\beta|}}{|\alpha-\beta|} \mathbf{1} \right] . \quad (79)$$

It is real, decreases exponentially at large distances, and locally vanishes as the product of the distance and the curvature for $|\alpha - \beta| \rightarrow 0$. When S consists of several disconnected pieces, the normals n_α on each of them should be oriented compatibly; for instance, all of them should point towards the outermost region. Along the integration path of (76), the series obtained by expanding $\ln(1 - K^2)$ in powers of K^2 converges. The values of $\Psi(y)$ at both ends of the integration path are given by (74) and (75).

The two terms of (76) correspond to the two different phenomena that we are studying. The first one is the *Casimir energy proper*, associated with the *variation of the zero-point energy* of the electromagnetic modes that is induced by the introduction of the perfectly conducting shells. It is the product of $\hbar c$ by a factor with dimension L^{-1} depending on the shape of S . The second one is the variation of the *free energy of the black-body* due to the effect of the boundaries on the gas of *real photons*. It has no ultraviolet divergence. The temperature T is that of the walls, which carry random currents in equilibrium with the quantized field.

When there are several material bodies, the surface S involves several disconnected sheets. One can then classify the various terms of the expansion of (78) in powers of K according to the position on these sheets of the scattering points α, β, \dots (Fig. 6). The terms for which all these points lie on the same connected sheet describe the free energy of *each separate body*; they do not contribute to the forces between indeformable bodies but determine internal constraints for thin conducting foils. Those for which some propagation $K(\alpha, \beta)$ occurs between two points α and β situated on different sheets describe the *interaction* free energy.

5.6 Conditions for the existence of the Casimir effect

We have proved above the existence of a limit F for the free energy of the field only, for perfectly conducting, thin walls, which defines the Casimir effect. This has been made possible under two conditions, which we now discuss.

On the one hand, the Casimir effect exists only owing to the *electromagnetic* nature of the field. Our proof made use of the cancellation of the one-scattering terms $\pm MK\mathbf{j}_0$ of the expansions (65) and (67), which eliminated a divergent surface contribution. Let us show that the *ultraviolet divergence* of (52) *cannot be removed for a scalar field*, so that the *specific features of electromagnetism are essential* to assign an energy to the field separately. Actually, the high-frequency expansion of the density of eigenmodes that replaces (50) for a scalar field includes, after a volume term $vq^2/2\pi^2$, an *area term* equal to $-sq/8\pi$ for Dirichlet boundary conditions (cancellation of the field at the wall), or to $+sq/8\pi$ for Neumann conditions (cancellation of the normal derivative), where s is the area of the boundary of the domain v . This term is associated with the occurrence of single scattering in the expansion analogous to (65). In the evaluation of the regularized free energy (52) the contributions of the two sides of the walls add up. A contribution

$\mp(\hbar cs/8\pi) \int_0^\infty dq q^2 \chi(q)$ proportional to the area s of the walls S occurs, and its divergence when the ultraviolet cutoff Q tends to infinity is incurable. A divergent Casimir force, tending either to stretch or to shrink the boundaries, would thus appear for a scalar field. The properties of matter interacting with the field could not be disregarded.

The inexistence of a divergent area term for the electromagnetic field can be traced to the mixed boundary conditions $\mathbf{E}_t = 0$, $(\text{curl}\mathbf{E})_n = 0$ and to the constraint $\text{div}\mathbf{E} = 0$. The first condition is of the Dirichlet type for the two tangential components of \mathbf{E} ; the constraint yields a Neumann boundary condition for the normal component. However the condition $(\text{curl}\mathbf{E})_n = 0$ relates the two tangential components to each other, so that altogether the electromagnetic field behaves as two scalar fields, one with Dirichlet, the other with Neumann boundary conditions. The fact that the area terms are opposite for these two boundary conditions entails their compensation.

A second condition is also necessary for the renormalization of the total Casimir energy, namely the *smoothness of the boundaries* S . We have relied, in our elimination of the ultraviolet divergence, on the behaviour (74) of $\Psi(y)$ for large y , which itself requires a *finite curvature* of S . To understand the origin of this condition, let us return to the expansion (50) of the eigenmode density $\rho^{(v)}$ for a given volume v . Its first term was cancelled by the subtraction $\rho^{(\Sigma)}$ in (52). The next curvature term of (50) yields in $F^{(v)}$, given by (49), a $\int q dq$ divergence. Fortunately, at each point α of the boundary S , the curvatures are opposite on the two sides of this boundary. Hence, in the summation over the domains v of (52), the curvature terms cancel one another. Accordingly, the large y expansion (74) of $\Psi(y)$ begins with a second order curvature contribution.

If, however, the surface S has a *sharp fold*, for instance if it is a hollow thin cube, this cancellation of the divergences from both sides S no longer occurs. The third, wedge term of (50) gives rise to the same $\int q dq$ divergence as the curvature term for each $F^{(v)}$. Let us evaluate its coefficient. Going from one side of the surface S to the other changes the dihedral angle θ into $2\pi - \theta$. The sum of the wedge contributions to $\delta\rho$ from the two neighbouring domains is thus

$$\frac{1}{12\pi^2} \int ds \left[\frac{(\pi - \theta)(\pi - 5\theta)}{\theta} + \frac{(\theta - \pi)(5\theta - 9\pi)}{2\pi - \theta} \right] = \frac{1}{6\pi} \int ds \frac{(\pi - \theta)^2}{\theta(2\pi - \theta)}, \quad (80)$$

and it is a positive number as soon as $\theta \neq \pi$. Hence F_{reg} is dominated by

a positive, divergent term proportional to (80), and the field exerts in this idealized model an infinite constraint on the considered foil, which tends to *flatten* its dihedron.

The same divergence occurs for an open conducting foil. Its *edge* is equivalent to a dihedral angle $\theta = 2\pi$, the contribution of which to $\rho^{(v)}$ is $(3/8\pi) \int ds$. The divergence of F implies, for instance, that the zero-point energy of the field produces a strong attractive force which tends to join the two halves of a thin conducting foil that is cut along a line.

We also find a divergence if S involves several adjacent dihedra, for instance, if it is made of three half-planes joined along their common edge as in a *honeycomb*. In this case, for $\theta = 2\pi/3$, we find a contribution to $\delta\rho$ equal to $(-7/24\pi) \int ds$ which is *negative*. Such a configuration would thus be particularly stable if the experiment could be realized.

The fact that one cannot define a finite Casimir energy for thin conducting foils with creases is related to the singularities of electromagnetic fields near sharp edges.

Nevertheless the above treatment can easily be adapted to Casimir forces between perfectly conducting *rigid bodies, even if they have sharp angles*. Consider, for instance, two bulky wedges. The free energy of each of them cannot be renormalized, because the kernel $K(\alpha, \beta)$ is singular as $1/|\alpha - \beta|^2$ for two neighbouring points α and β located on the different sides of the edge; the resulting contribution $\text{Tr}K^2$ to (78), in particular, is seen to generate a divergence in (76). If, however, according to the remark at the end of section 5.5, we focus on the interaction between the two indeformable wedges, letting aside their own energies, such divergent contributions are irrelevant. The interaction free energy of the two wedges is thus obtained by keeping, in the expansion of (78) in powers of K , only those terms which involve scatterings on both wedges (with an even number of factors K). Their contribution to (76) is expected to be finite in spite of the short-distance singularity of K near the edges of the wedges, and the Casimir force between them is therefore well defined. For example, for two wedges with the same dihedral angle 2θ facing each other perpendicularly at a distance L , the two-scattering approximation expressed below by eq.(92) provides at $T = 0$ an attractive Casimir interaction energy equal to $-\hbar c \text{tg}^2\theta/4\pi^2L$.

We now review some applications of the general expression (76) for the Casimir free energy. More details can be found in [18].

6 Applications

6.1 Parallel plates

For two parallel plates with area \mathcal{A} , lying at a distance L from each other, the function $\Psi(y)$ associated with the three regions separated by these plates is

$$\Psi(y) = \frac{\mathcal{A}y^2}{2\pi} \ln(1 - e^{-2yL}) , \quad (81)$$

wherefrom we get the elementary Casimir effect at $T = 0$. The low temperature expansion of the free energy (76),

$$F(T) = -\frac{\mathcal{A}\pi^2\hbar c}{720 L^3} - \frac{\mathcal{A}T^3\zeta(3)}{2\pi \hbar^2 c^2} + \frac{\mathcal{A}\pi^2 L T^4}{45\hbar^3 c^3} + \mathcal{O}(T^2 e^{-\pi\hbar c/LT}) , \quad (82)$$

agrees with the result (37) of the direct calculation, and shows that the Casimir attraction $-\partial F/\partial L$ increases with the temperature.

The comparison of (70), which includes the factor $\ln(1 - e^{-\hbar c q/T})$, with (76), (81), exhibits a *duality between high and low temperatures*, as anticipated in Eqs (34), (38) and (39),

$$F(T) - F(0) = \left(\frac{2LT}{\hbar c}\right)^4 \left[F\left(\frac{\hbar^2 c^2}{4L^2 T}\right) - F(0) \right] . \quad (83)$$

At high temperature, we have

$$F(T) = -\frac{\mathcal{A}T \zeta(3)}{8\pi L^2} + \mathcal{O}(T^2 e^{-4\pi LT/\hbar c}) , \quad (84)$$

yielding again an attraction due to radiation pressure.

The *entropy* $-\partial F/\partial T$ rises at low temperatures as $3\mathcal{A}T^2\zeta(3)/2\pi\hbar^2 c^2$, independently of the distance between the plates, and tends to a *finite* limit $\mathcal{A}\zeta(3)/8\pi L^2$ at high temperature.

6.2 Low temperatures

Owing to the more and more rapid oscillations of $g(y)$ when $T \rightarrow 0$, we can evaluate the second term of (76) for low temperatures by expanding $\Psi(y)$ around $y = 0$. This yields

$$F(T) - F(0) = \frac{\pi T^2}{3\hbar c} \Psi'(0) - \frac{\pi^3 T^4}{135\hbar^3 c^3} \Psi'''(0) + \mathcal{O}(T^6) . \quad (85)$$

This behaviour is related to the *topology* of the boundaries S , since according to (75) $\Psi'(0)$ vanishes for a singly connected surface, and equals nA for a multiply connected surface. Accordingly, the low-temperature *entropy* arising from (85) behaves for $n = 0$ as T^3 (like the entropy of the black body), but is large as $-2\pi n AT/3\hbar c$ for $n \neq 0$. This negative sign looks paradoxical. It is related to the fact that for torus-like topologies, permanent supercurrents can generate *static magnetic fields*. The occurrence of a number $2n$ of such modes with $q = 0$, which do not contribute to the Casimir effect, entails a depletion in the distribution $\rho^{(v)}(q)$ for $q \neq 0$. In fact, we see from (69), (71), (75) that $\delta\rho(q)$ for $\Sigma \rightarrow \infty$ tends to $-2nA/\pi$ as $q \rightarrow 0$; it is this negative sign which is reflected in that of the Casimir entropy. However the total entropy of a quantum system must be positive. In the present case this results from the positivity of the total density of eigenmodes $\sum_v \rho^{(v)} = \rho^{(\Sigma)} + \delta\rho$ of the field, ensured by the fact that $\rho^{(\Sigma)} \sim Vq^2/\pi^2$ is infinite in the large Σ limit considered here.

The dimensionless parameter of the expansion (85) is $\ell T/\hbar c$ where ℓ is the typical size of the system S . The lowest order contributions should become experimentally accessible since this parameter is 0.5 for $T = 300\text{K}$ and $\ell = 3\mu\text{m}$.

The different behaviour of (82) and (85) arises from the fact that (85) holds only for a finite system, whereas for an infinite system like a pair of parallel plates $\Psi'''(y)$ diverges when $y \rightarrow 0$ as shown by (81).

6.3 High temperatures

At high temperature the second term of (76) is dominated by the first saw-tooth of $g(y)$. The corresponding calculation yields

$$F = -CT \ln(T/\hbar c Q) + \mathcal{O}(T^{-1}) , \quad (86)$$

$$C = \Psi(+0) - \Psi(\infty) = \frac{1}{32\pi} \int_S d^2\alpha \left(\frac{3}{R^2} - \frac{1}{R_1 R_2} \right) - n , \quad (87)$$

$$\ln Q = -\frac{1}{C} \int_0^\infty dy \ln y \Psi'(y) . \quad (88)$$

Here the dimensionless parameter $\hbar c/TR$ of the expansion (86) is governed by a length R of the order Q^{-1} associated with the short-range behaviour of the kernel K . This characteristic length is therefore a typical curvature

radius R of S . The high-temperature limit might become experimentally relevant for crippled foils with small R .

The dominant term of (86) is formally the same as the free energy (47) of a number \mathcal{C} of *classical harmonic oscillators* with average frequency $c\mathcal{Q}/2\pi$. Contrary to what happens for the black-body which requires a quantum treatment at any temperature, the Casimir contribution that we have calculated, which describes the change in the free energy of photons brought in by the boundaries S , takes a *classical* form for $T \gg \hbar c/R$. This is possible here because the modes that contribute to the Casimir effect have bounded frequencies, whereas the modes with $h\nu \gg T$ crucially contribute to the black-body radiation.

The internal energy $U \sim \mathcal{C}T$ arising from (86) expresses the classical *equipartition*, and as usual in the classical limit the entropy $\mathcal{C} \ln(eT/\hbar c\mathcal{Q})$ depends on Planck's constant in its additive constant. The number \mathcal{C} , positive or negative, is interpreted as the *average number of modes* with finite frequency *added by the introduction of the boundaries S* . Here again the *topology* of S enters the expression (87) of \mathcal{C} through the genus n and the integer $\int d^2\alpha/4\pi R_1 R_2$. For parallel plates, we have $\mathcal{C} = 0$ but $\mathcal{C} \ln \mathcal{Q} = -\mathcal{A} \zeta(3)/8\pi L^2$.

The high-temperature Casimir *constraints* on the conductors S describe the effects of *radiation pressure*. To dominant order they behave as $T \ln T$ and are obtained by studying how \mathcal{C} varies when the conductors are displaced or deformed. They tend to let F decrease, thus to let \mathcal{C} increase. The only non-topologic part of \mathcal{C} , $3 \int d^2\alpha/(32\pi R^2)$, does not depend on the relative position of the conductors. Hence, to the dominant order in $T \ln T$, there are no forces between different conductors induced by the field. Moreover, since \mathcal{C} is dimensionless and scale-invariant, there are no there forces tending to dilate or contract hollow conducting shells. However \mathcal{C} increases with the average curvature $1/R$ of S , so that the Casimir effect tends at high temperature to *let conducting foils undulate*. This tendency is limited by the next terms of the expansion (86), and the curvature $|R|^{-1}$ tends to rise up to values of order $T/\hbar c$.

The next order contributions to the constraints, of order T , arise from the contribution $\mathcal{C}T \ln \mathcal{Q}$ to F . Since \mathcal{Q}^{-1} is proportional to the size of S , these Casimir forces of order T would tend to contract S if \mathcal{C} is negative, to expand it if \mathcal{C} is positive.

6.4 The wrinkling effect

The existence of constraints that tend to wrinkle conducting surfaces at high temperature is confirmed by the study of *small deformations of a thin foil*. The evaluation of (76) for a weakly deformed conducting plane S is achieved by means of a two-dimensional Fourier analysis. It is found that the constraints created by the field tend to create ripples with wavelengths larger than $2.9\hbar c/T$, and to restore flatness for smaller wavelengths. In particular, the Casimir effect proper, at zero temperature, tends to suppress the curvatures. Thus a *conducting plane foil is stable at $T = 0$, but unstable at $T \neq 0$* under small deformations.

This phenomena is confirmed by the study of the *distribution in space of the free energy* of the electromagnetic field. The density of Casimir free energy $f(r)$ is obtained in the same way as the total free energy (76), except for the integration over the point (68). In fact, taking into account the spectral representation (61) of the magnetic Green function $\mathbf{\Gamma}$ and the similar one for the electric function $\mathbf{\Xi}$, the contribution of each pole $k = q_m$ of $\Phi^{(v)}(k)$ is then weighted by $\frac{1}{2}[\mathbf{B}_m^2(r) + \mathbf{E}_m^2(r)]$. (The coefficients μ_0^{-1} and ϵ_0 of (2) are recovered when the physical fields entering (45) are expressed in terms of the real and normalized functions entering $\mathbf{\Gamma}$ and $\mathbf{\Xi}$.) The density of free energy $f(r)$ is thus found as a series describing a wave starting from r , scattering an even number of times on S and returning to r . The two-scattering term is sufficient to provide the free energy density at a point r located near S , at a distance d from it much shorter than the local curvature radii. We find at low temperature

$$f(r) = -\frac{\hbar c}{30\pi^2 R d^3} + \frac{T^3 \zeta(3)}{2\pi R \hbar^2 c^2} + \dots, \quad (89)$$

and at high temperature

$$f(r) = \frac{T}{16\pi R d^2} \left[\ln(2dT/\hbar c) + C - \frac{1}{4} \right] + \dots, \quad (90)$$

where C is Euler's constant.

This density is not bounded when $d \rightarrow 0$, and its divergence is non-integrable. Hence, even after renormalization by subtraction of the free energy of the vacuum without boundaries, the free energy $F^{(v)}$ associated with *each region* is *divergent*. The total free energy $F = \sum_v F^{(v)}$ is finite because

on the two sides of S the average curvatures R^{-1} are opposite at each point, so that the divergences from (89) or from (90) cancel each other.

The sign in (89) shows that the presence of a perfectly conducting foil produces the transfer of an *infinite* amount of *zero-point energy from the concave to the convex side*, whereas, according to (90), the energy of *real photons* is transferred *from the convex to the concave side*. These opposite signs are consistent with the stability or unstability of a plane foil against deformations, depending on the temperature.

6.5 Other examples

6.5.1 Van der Waals and Casimir-Polder forces.

The Casimir forces between conductors lying *far apart* can be evaluated by means of the free energy (76) of the vacuum separating them. We noted that it may also be attributed to the *random currents* that circulate on their surface and produce the field. Such forces have thus the same nature as *van der Waals forces* of mutual induction, except for the retarded character of the interaction. We find from (76) that two conductors at a large distance L apart *attract* each other as $1/L^8$ at zero temperature (Casimir-Polder forces [3]), as T/L^7 at high temperature (van der Waals forces). *Torques* are also found for anisotropic bodies. The same results hold for a small conducting body facing a mirror, which is attracted by it [31].

6.5.2 Derjaguin approximation.

For two *neighbouring conductors*, the multiple scattering expansion of (78) can be used to justify the *Derjaguin approximation* seen above. Consider for instance the Casimir force between a plane and a sphere with radius R , and denote by L their shortest distance (Fig. 7). The trace in (78) can be replaced by an integration over a point α of the plane:

$$\Psi(y) = -\frac{1}{4} \int d^2\alpha \, y \frac{d}{dy} [\text{tr} \ln(1 - K^2)]_{\alpha\alpha} , \quad (91)$$

where the trace tr is meant on the tensor index only. Suppose $L \ll R$. Owing to the exponential decrease of K , the integral (91) is dominated by the contributions such that α lies at a distance x from the sphere of order L , and such that all successive scattering points also lie at a distance of order

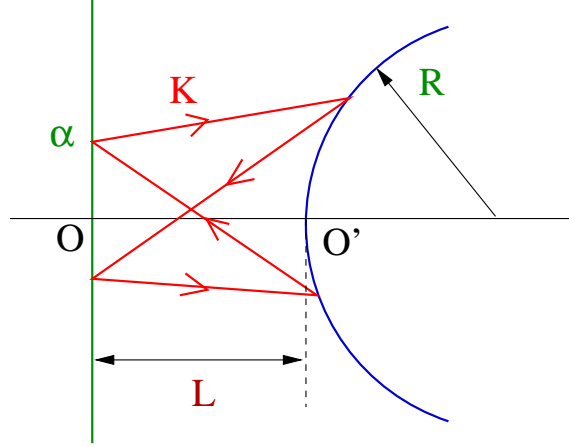


Figure 7: Multiple scattering contributing to the characteristic function Ψ (91).

L from α . Thus, for each α , the integrand of (91) is approximately the same as for two parallel plates lying at a distance x apart, which according to (81) is given by $\pi^{-1}y^2 \ln(1 - e^{-2yx})$. This is just Derjaguin approximation. Corrections can be obtained from (91).

6.5.3 Two-scattering approximation.

Another useful approximation is the *two-scattering approximation*, for which we retain for $\Psi(y)$ only the lowest order term $\frac{1}{2}\text{Tr}Kydk/dy$ of (78). More explicitly, this yields (Fig. 8)

$$\begin{aligned} \Psi^{(2)}(y) &= 2y \frac{d}{dy} \int d^2\alpha d^2\beta \frac{dG_0(|\alpha - \beta|)}{dn_\alpha} \frac{dG_0(|\alpha - \beta|)}{dn_\beta} \\ &= -\frac{y^2}{8\pi^2} \int d^2\alpha d^2\beta (n_{\alpha \cdot \rho})(n_{\beta \cdot \rho}) \frac{1}{\rho} \frac{d}{d\rho} \frac{e^{-2y\rho}}{\rho^2} \end{aligned} \quad (92)$$

where ρ is the vector $\alpha - \beta$. Numerical tests show that this approximation should be fairly good; for example it yields for the Casimir force at $T = 0$ between two parallel plates the correct result times $90/\pi^4$, an error of 8%.

Using this approximation, we can evaluate the free energy of interaction between a plane and a sphere. The integrals in (92) can be completely worked

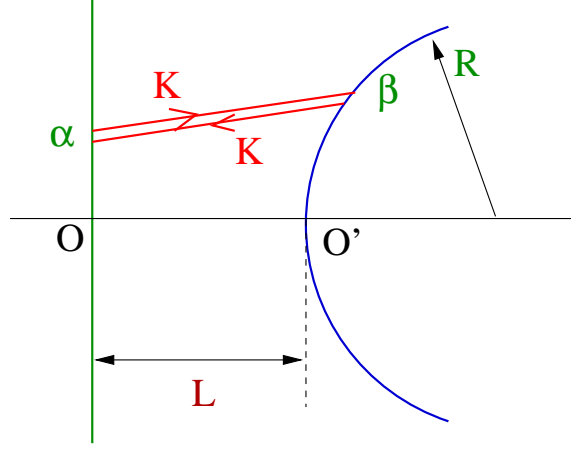


Figure 8: Geometry of the two-scattering approximation (92).

out and yield

$$\Psi^{(2)}(y) = \left(-\frac{1}{2}Ry + \frac{1}{4}\right) e^{-2yL} - \left(\frac{1}{2}Ry + \frac{1}{4}\right) e^{-2yL-4yR}. \quad (93)$$

Hence we find at $T = 0$, for $L \ll R$,

$$E^{(2)} \approx -\frac{\hbar c R}{8\pi L^2} + \frac{\hbar c}{8\pi L}, \quad (94)$$

which exhibits a correction in L/R to the two-scattering Derjaguin contribution.

The study of a *spherical shell* S with radius R shows that the Casimir energy at $T = 0$ behaves as [33, 18, 34]

$$E = 0.046 \hbar c / R. \quad (95)$$

At high temperature, we find in agreement with (86)

$$F = -\frac{T}{4} [\ln(TR/\hbar c) + 0.769] - \left(\frac{\hbar c}{R}\right)^2 \frac{1}{3840T} + \mathcal{O}\left(\frac{1}{T^3}\right). \quad (96)$$

In the previous examples we had found attractive Casimir forces. In contrast, these forces tend here at any temperature to *expand the sphere*. They increase

with T . The radiation pressure exerted from inside thus exceeds that exerted from outside, contrary to what happens for parallel plates.

An intermediate geometry between a sphere and parallel plates is that of a *cylinder*. We evaluate the Casimir energy of a hollow cylinder S by means of the two-scattering approximation (92). For a cylinder with radius R and length $\mathcal{L} \gg R$, we find at low temperature

$$F^{(2)} \sim -\frac{2\pi^3}{45 \hbar^3 c^3} \mathcal{L} R^2 T^4, \quad (97)$$

and at high temperature

$$F^{(2)} \sim -\frac{3}{64} \frac{\mathcal{L}}{R} T \ln \frac{4.56 TR}{\hbar c}, \quad (98)$$

in agreement with (86). The cylinder tends to shrink at high temperature. At zero temperature, the zero-point energy *vanishes* in the considered approximation and its exact value is very small, an intermediate situation between the parallel plates (82) and the sphere (95).

Unfortunately all these Casimir constraints on thin conducting foils, including the wrinkling effect, are presently difficult to detect experimentally, because of their weakness compared to the binding forces that ensure the cohesion of the metallic sheets.

References

- [1] Planck M 1901 *Ann. d. Phys.* **4** 553-563
- [2] Casimir H B G 1948 *Proc. Kon. Nederl. Akad. Wetensch.* **B51** 793-795
- [3] Casimir H B G and Polder D 1948 *Phys. Rev.* **73** 360-372
- [4] Sarlemijn A and Sparnaay M J 1989 *Physics in the Making* (Amsterdam: North Holland)
- [5] Lamoreaux S K 1997 *Phys. Rev. Lett.* **78** 5-8; 1998 *ibid* **81** 5475-76
- [6] Mohideen U and Roy A 1998 *Phys. Rev. Lett.* **81** 4549-52
- [7] Bordag M, Mohideen U and Mostepanenko V M 2001 *Phys. Rep.* **353** 1-205

- [8] *Vacuum Energy*, Poincaré Seminar 2002, ed B Duplantier and V Rivasseau 2003 (Basel: Birkhäuser Verlag)
- [9] Harris B W, Chen F and Mohideen U 2000 *Phys. Rev. A* **62** 052109(5)
- [10] Chan H B *et al* 2001 *Science* **291** 1941-44
- [11] Bressi G, Carugno G, Onofrio R and Ruoso G 2002 *Phys. Rev. Lett.* **88** 041804(4)
- [12] Chen F *et al* 2002 *Phys. Rev. Lett.* **88** 101801(4)
- [13] Chen F *et al* 2002 *Phys. Rev. A* **66** 032113(11)
- [14] Emig T *et al* 2003 *Phys. Rev. A* **67** 022114(15)
- [15] Genet G *et al* 2003 arXiv:quant-ph/0302071
- [16] Chen F *et al* 2003 *Phys. Rev. Lett.* **90** 160404(4)
- [17] Balian R and Duplantier B 1977 Electromagnetic waves near perfect conductors, I. Multiple scattering expansions and distribution of modes, *Ann. Phys. NY* **104** 300-335
- [18] Balian R and Duplantier B 1978 Electromagnetic waves near perfect conductors, II. Casimir effect, *Ann. Phys. NY* **112** 165-208
- [19] *Long-Range Casimir Forces* ed Levin F S and Micha D A 1993 (New York: Plenum Press)
- [20] Milonni P W 1994 *The Quantum Vacuum* (San Diego: Academic Press)
- [21] Mostepanenko V M and Trunov N N 1997 *The Casimir Effect and its Applications* (Oxford: Clarendon Press)
- [22] Elizalde E *et al.* 1994 *Zeta Regularization Techniques with Applications*, (Singapour: World Scientific)
- [23] Krech M 1994 *The Casimir Effect in Critical Systems* (Singapour: World Scientific)
- [24] J Brankov J G, Danchev D M and Tonchev N S 2000 *Theory of Critical Phenomena in Finite-Size Systems* (Singapour: World Scientific)

- [25] Milton K A 2001 *The Casimir effect: physical manifestations of zero-point energy* (Singapour: World Scientific)
- [26] Fierz M 1960 *Helv. Phys. Acta* **33** 855-858
- [27] Mehra J 1967 *Physica* **37** 145-152
- [28] Brown L S and Maclay G J 1969 *Phys. Rev.* **184** 1272-79
- [29] Derjaguin B 1934 *Kolloid Z.* **69** 155-164
- [30] Lambrecht A and Reynaud S in ref. [8]
- [31] Aspect A and Dalibard J in ref. [8]
- [32] Dembowski C *et al* 2002 *Phys. Rev. Lett.* **89** 064101(4)
- [33] Boyer T H 1968 *Phys. Rev.* **174** 1764-76
- [34] Cognola G, Elizalde E and Kirsten K 2001 *J. Phys. A* **34** 7311-27